Measuring the performance of a novel fluid film bearing supporting a rotor on a stationary shaft, by non-contacting means

Journal Item

Measuring the performance of a novel fluid film bearing supporting a rotor on a stationary shaft, by non-contacting means

J K Martin
Department of Environmental and Mechanical Engineering, The Open University, Walton Hall, Milton Keynes, Bucks MK7 6AA, UK

Abstract: A description is given of a multi-body dynamics rig for testing a novel rotor fluid film bearing system. The design included a composite rotor supported on a stationary central shaft, with loading applied by non-contacting electromagnets. The shaft included hydrostatic bearing pockets and continuously adjustable hydrodynamic bearing segments. A technique is described for deriving displacement coefficients for both types of bearing. Observations are given on the use of the rig and test techniques, along with some results, and on implications of the results regarding the bearing system.

Keywords: performance measurement, fluid film bearing, rotor

NOTATION

a_{pp}	direct displacement coefficient, force p, displacement p
a_{pq}	cross-displacement coefficient, force p, displacement q
a_{qp}	cross-displacement coefficient, force q, displacement p
a_{qq}	direct displacement coefficient, force q, displacement q
a_{xx}	direct displacement coefficient, force x, displacement x
a_{xy}	cross-displacement coefficient, force x, displacement y
a_{yx}	cross-displacement coefficient, force y, displacement x
a_{yy}	direct displacement coefficient, force y, displacement y
C_{r}	radial clearance with a concentric rotor
F_{L}	test rig electromagnet force, left hand
F_p	incremental load on the rotor, p axis component
F_q	incremental load on the rotor, q axis component
F_{R}	test rig electromagnet force, right hand
F_X	rotor load, X component
F_Y	rotor load, Y component
F_1	incremental load applied to the rotor
F_2	incremental load applied to the rotor
O'	rotor centre equilibrium position for a known load
p, q	local axes, variable orientation, not necessarily perpendicular
W	rotor load
x, y	local axes, variable orientation, perpendicular
X, Y	fixed global axes, perpendicular
α	angle between the x, y and X, Y axis sets
γ	angle between the X and p axes
ΔT	lubricant temperature rise
θ	angle between the x and p axes $= \gamma - \alpha$
ϕ	angle between the x and q axes $= \psi + \gamma - \alpha$
ψ	angle between the p and q axes

The MS was received on 20 February 2003 and was accepted after revision for publication on 27 April 2004.

1 INTRODUCTION

A novel form of adjustable fluid film bearing has hydrodynamic characteristics that can be changed in a continuously controlled manner during operation [**1**]. The principle can be applied to conventional journal bearings, i.e. a shaft or journal rotating within a stationary housing, to inverse orientations, i.e. a rotor on a stationary shaft, and to thrust bearings. The continuous adjustment capability was first demonstrated on the test rig containing a bearing system of the inverse orientation type. No published work could be found reporting practical experiments for fluid film bearings of this inverse orientation arrangement, or on the adjustment concept.

The test rig was designed to measure bearing performance for both rotating and non-rotating modes by adapting

recently devised measurement techniques. Forces were applied to the rotor, and its displacements sensed, by non-contacting means. This paper describes the design of the test rig and its operating principles, giving some illustrated test results and observations on its use.

The main testing operations comprised the following:

(a) provision of known bearing loads to the rotor in a range of directions, together with the ability quickly to change the magnitude and/or direction of the load;
(b) indication of the position, and changes in position, of the centre of rotation of the rotor for all test conditions;
(c) provision of data suitable for deriving bearing displacement coefficients for a range of test conditions.

Fluid film bearing performance is often described in terms of four displacement coefficients and four velocity coefficients. These are grouped to represent net oil film forces arising from lateral displacements and velocities of the rotating member produced by the load and changes in load. Many authors simply refer to those coefficients arising from displacements as 'stiffness coefficients' and those from velocities as 'damping coefficients', being indicators of bearing stiffness and damping respectively. Others, particularly when investigating the behaviour of rotating systems, prefer the more generic and less commital terms 'displacement' and 'velocity' coefficients [**2**]. For this work the generic terms have been used, but to all intents and purposes the term 'displacement' coefficient can be considered equally as 'stiffness' coefficient, giving an indication of the stiffness of the novel bearing.

2 BEARING AND ROTOR SYSTEM

The bearing and rotor system simulated a proposed design of grinding machine tool spindle and grind-wheel mounting arrangement [**3**]. The grind-wheel (i.e. rotor) was belt driven and supported by fluid film bearings on a stationary central shaft or stator. There were two hydrodynamic bearings of the novel adjustable configuration, separated along the shaft, and a single four-pocket hydrostatic bearing in between. The purpose of the hydrostatic bearing was to support the rotor for zero speed and all other conditions when the hydrodynamic bearings were not operating. The same oil was used for all bearings. Figure 1 shows a longitudinal cross-section of the rotor and shaft arrangement.

The steel shaft had a nominal diameter of 70 mm and housed the hydrostatic bearing pockets, their feeds and restrictors, the hydrodynamic bearings, their oil feeds, adjustment devices and a combined scavenge oil return. Figure 2 depicts the shaft used. Oil supply was via end blocks containing galleries and O ring seals to minimize pipework and allow efficient access to the adjuster controls and other items.

There were four adjustable segments associated with each hydrodynamic bearing, each controlled by a steel adjuster pin. Each adjuster pin comprised a small location diameter,

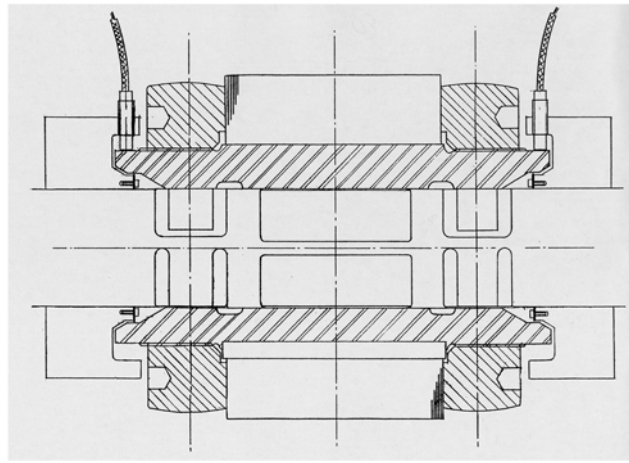

Fig. 1 Rotor cross-section

a tapered support length, engagement thread and a square end for locating a key. The tapered portion bore against the under surface of the adjustable segment, providing a radially stiff load path. Turning the adjuster caused a longitudinal wedging action. The effect was to lift or lower the segment surface slightly in a controlled and continuous manner, thereby changing the hydrodynamic conditions, irrespective of any loads. This concept and the effect on the hydrodynamic action have been reported [**4**].

The rotor is shown in Fig. 3. It was of composite construction and designed to interact with large adjacent electromagnets positioned schematically as in Fig. 4. The rotor core comprised a central steel collar upon which were keyed a large number of steel disc blanks, each 0.65 mm thick. These provided the majority of the interaction between the rotor and the electomagnets and were of the BS-specified power loss rating of 10 W/kg at 1.5 T 50 Hz [**5**]. They were clamped by large nuts threaded to the rotor collar doubling as crowned pulleys for drive belts. The nuts in turn were locked in place with keyed lock rings and aluminium belt guides, visible in Fig. 3, which doubled as shields against possible electromagnetic interference (EMI) effects

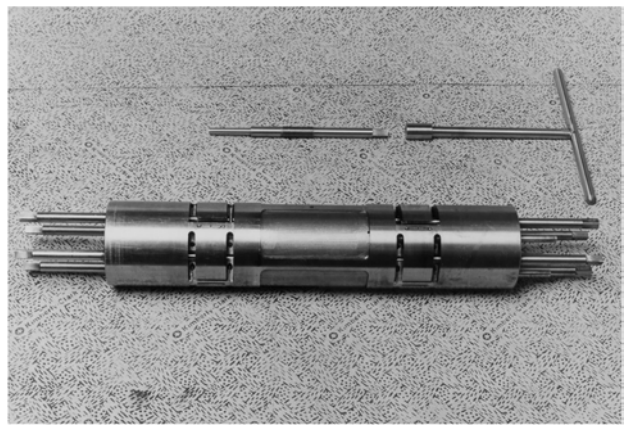

Fig. 2 Central shaft assembly

Fig. 3 Rotor assembly

from the magnets. The bore of the rotor inner collar was lined with a BS grade A tin-rich white metal [**6**], approximately 1 mm thick and machined to a constant diameter throughout the axial length. The outer surface of the rotor was finish ground to circularity and parallelism tolerances well within 5 μm. The complete rotor mass was 38.3 kg.

In the axial direction the rotor was a 1 mm clearance fit between the end mounting blocks which clamped and supported the shaft. Low-friction thrust bearing faces abutted the ends of the rotor collar in the event of any extreme longitudinal motions. The drive belt tensions themselves could be quickly zeroed and restored, before and after taking individual test readings. When such readings were taken, the rotor was supported solely by a combination of the bearing oil film forces in four degrees of freedom, with only the oil film shear resisting its high angular momentum. There were no oil seals other than non-contacting shields and guides, to avoid influencing bearing forces.

3 ELECTROMAGNET LOADING SYSTEM

Two large electromagnets were specially made, each as a large coil embedded in a block of resin. They each provided up to a rated 1 kN static attraction force, drawing 40 A at 10 V. The main aspect affecting the capacity of the electro-magnets was the constancy of applied force across the gap between the magnet face and rotor. The larger (and heavier) the magnet, the lesser this was affected by changes in the gap distance. The design chosen produced a constant force for a gap of between 0 and approximately 5 mm.

Each electromagnet was mounted in a cradle which could be positioned at a range of angles from 0 to 90° individually, or 0 to 45° both together. Figure 5 shows both cradles set horizontally at zero. Each electromagnet was located by light linkages and self-aligning ball bearing assemblies. These comprised a low-friction mechanism which allowed only one degree of freedom of motion of the magnet in a direction radial to the rotor assembly, at whatever angle the cradle was set. A load cell in this path read the electromagnetically applied force, combined with any weight component. Each electromagnet was energized by a single-phase variable transformer unit. Rotary control potentiometers allowed each magnet force to be changed smoothly and continuously and held at any required value within range. Resolution was ± 0.1 kgf throughout the range.

Each whole cradle assembly was located on two circular mountings set concentrically with the central shaft to provide the series of angular positions from horizontal to vertical. Alternatively, setting both magnets at the same angle of 22.5° above horizontal, as shown in Fig. 4, allowed a load equivalent to the rotor weight to be vectored in virtually any radial direction by suitable adjustment of the magnet forces, without the need for physical repositioning.

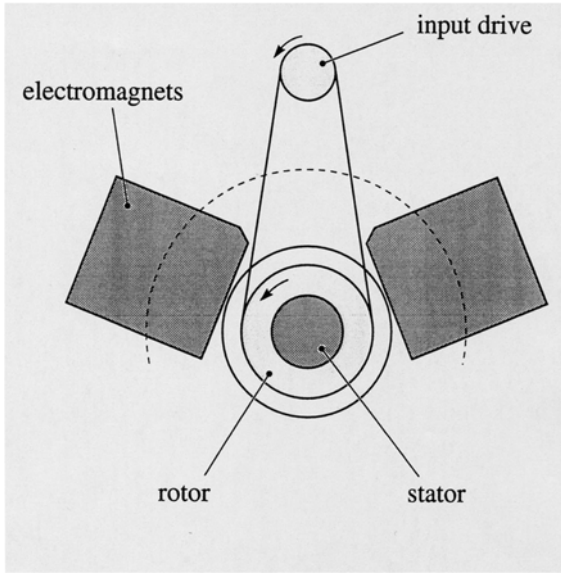

Fig. 4 Electromagnet positioning

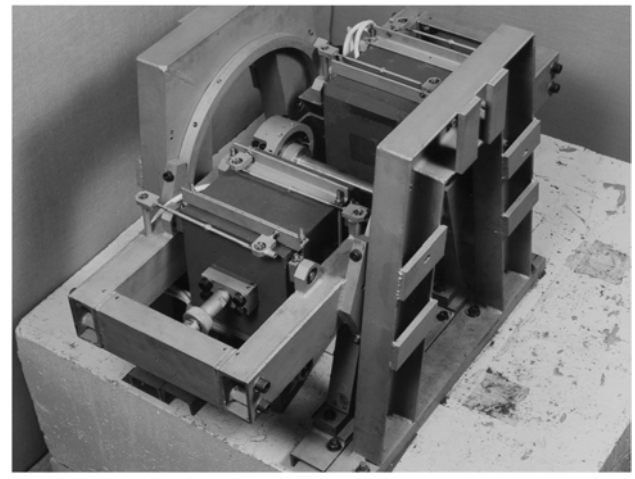

Fig. 5 Electromagnet and cradle assemblies

4 MAIN TEST RIG SYSTEMS

Figure 6 shows an overall view of the complete test rig, with the magnets set at 22.5° above horizontal. The rotor drive power was supplied by a variable-speed three-phase d.c. motor rated at 4 kW at 3000 r/min. Mechanical power was transmitted by flat synthetic leather belts and crowned pulleys. The rotational drive speed was geared upwards by pulley diameter ratios in two stages to provide a rotor maximum of 7000 r/min. All rotating parts were dynamically balanced.

The bearing lubricant was a straight mineral oil of viscosity ISO VG 32 containing some anticorrosion and de-emulsifying additives. The oil supply system comprised three main parts: the hydrostatic supply circuit, hydrodynamic supply circuit and scavenge return. A main reservoir tank served all parts. All pipes connected to the shaft included flexible lengths to isolate any pump vibrations. Pressure for each supply circuit was independently set with reducing valves, with isolator valves then controlling final admission to the relevant circuit. System pressures were monitored using conventional Bourdon-type gauges.

Scavenged oil returned to the main reservoir via an oil cooler and filter. Oil flowrates were determined by timed collection measurements. Four contact thermocouples indicated temperatures of the oil in the main tank, hydrodynamic feed, hydrostatic feed and central gallery output. In addition, a roving thermocouple head could be positioned through access holes to record the temperature of oil on immediate exit of the hydrodynamic bearings.

The instrumentation system is shown outlined in Fig. 7. Rotor radial displacement was sensed by four non-contacting inductive type transducers mounted in pairs orthogonally at each end. One of each pair is visible in Fig. 1. The gaps, and changes in gap, between the ends of the transducers and adjacent rotor surface were sensed. Outputs were low-voltage d.c. signals fed to digital voltmeters and an oscilloscope which provided a summative visual indication of the position and locus of the rotor centre of rotation. The main advantage of this inductive type of transducer is that it is not affected by the varying presence of any oil in the gap. The main disadvantage, based on experience with a variety of different sizes and types, is that during an experiment the effective position of the electrical origin may drift over a period of time. Characteristic gradients, however, tend to be stable for a variety of test temperatures and conditions and over time, so relative displacements are reliable. Test techniques were therefore used that involved measuring and processing changes in rotor displacements, irrespective of the electrical origin position. Possible EMI effects from the electromagnets were checked by locking the rotor firmly in position and applying ranges of steady and transient electromagnet forces. None was apparent. The keyway for the rotor laminations doubled as a signal spike trigger for sensing rotor speed with a multimeter counter.

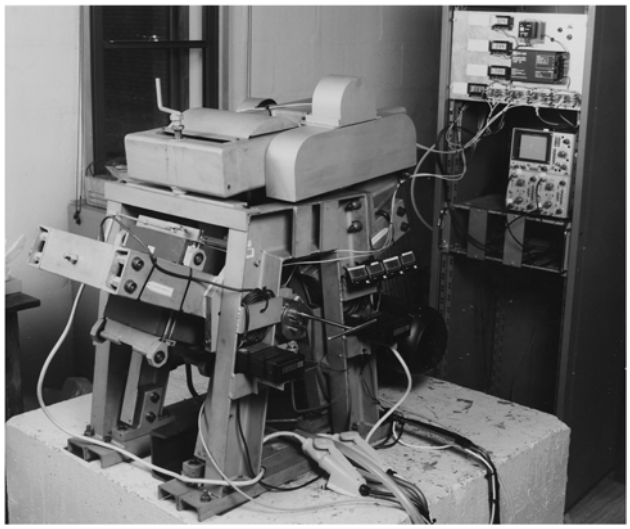

Fig. 6 Main test rig assembly

5 MEASUREMENT TECHNIQUES

A method of measuring displacement coefficients was adapted from an extended selected orbit technique reported by Parkins [**7**]. This reported method was for measurements of velocity coefficients based on the generation of journal orbits containing overlapping straight lines over part of their length. The technique involved the use of the overlap portions and an accompanying coordinate system, the axes of which aligned with the straight-line parts of the orbits, but which, although non-parallel, were not of necessity perpendicular. Velocity coefficients were computed in relation to this (p, q) axis set and subsequently converted to those based on any desired coordinate system, such as perpendicular axes x, y, with y aligned with the load direction. The advantages of this extended technique included the relative ease of generating suitable orbits and, aided by recent developments in data acquisition methods, the yielding of all four velocity coefficients from the same single orbit.

The method was adapted to the measurement of rotor displacement coefficients in conjunction with an incremental load technique. Figure 8 shows the basis of this adapted technique. The rotor was assumed to be rotating at a steady speed about the rotational centre O' under the influence of a known constant load. An incremental load, F_1, was applied to the rotor, causing it to move a distance p to new equilibrium position 1. The incremental load F_1 was then removed and another one, F_2, was applied in a different direction, resulting in new equilibrium position 2, a distance q from O'. Incremental loads were set by appropriate adjustments of the magnet forces F_L and F_R which, when combined with the rotor load, W, produced the required resultant incremental force. Loads F_1 and F_2 were chosen so as to make ψ a reasonable size.

The coordinates of points O', 1 and 2 could be determined from transducer measurements and represented as (X_0, Y_0),

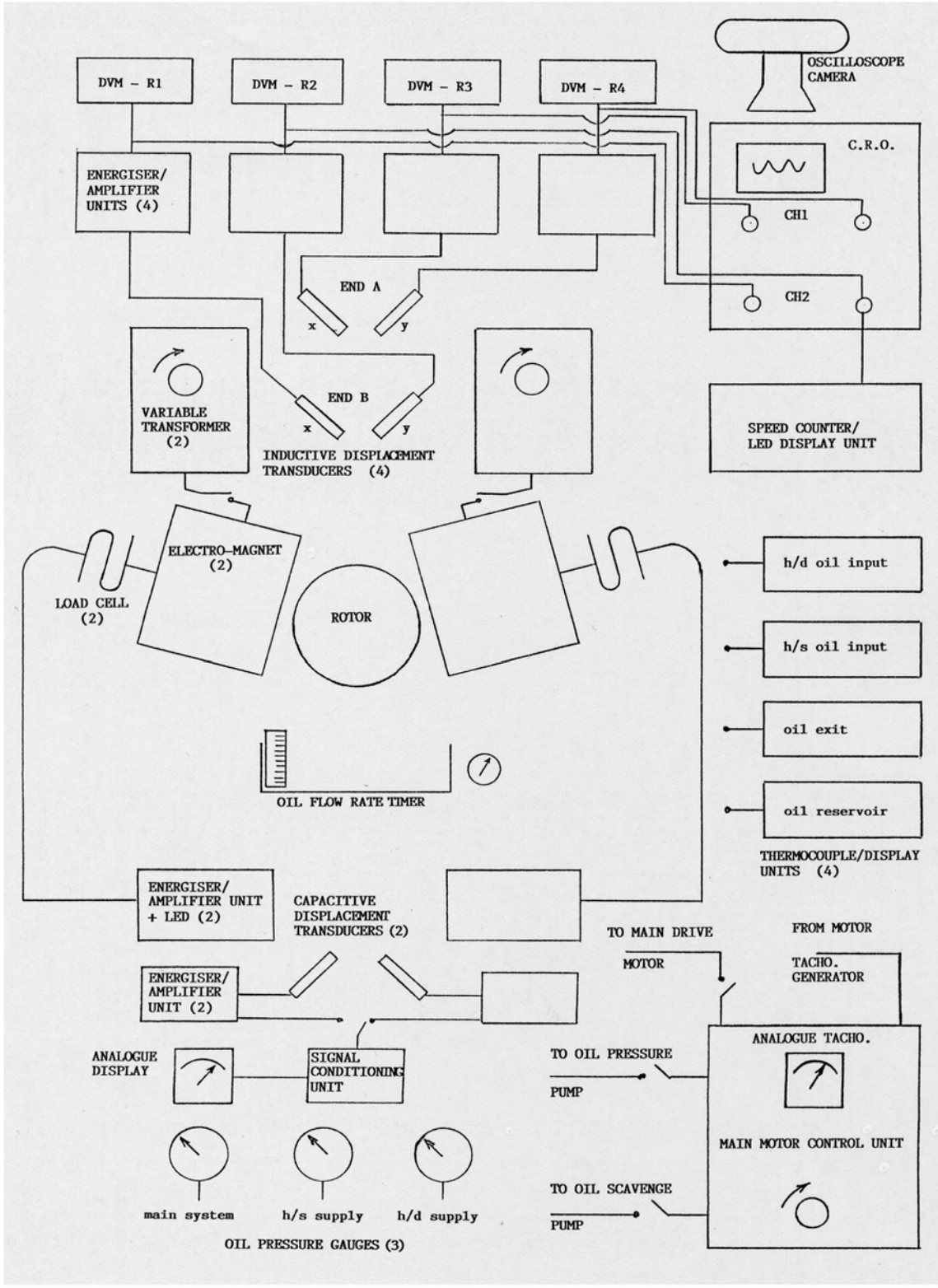

Fig. 7 Instrumentation—outline

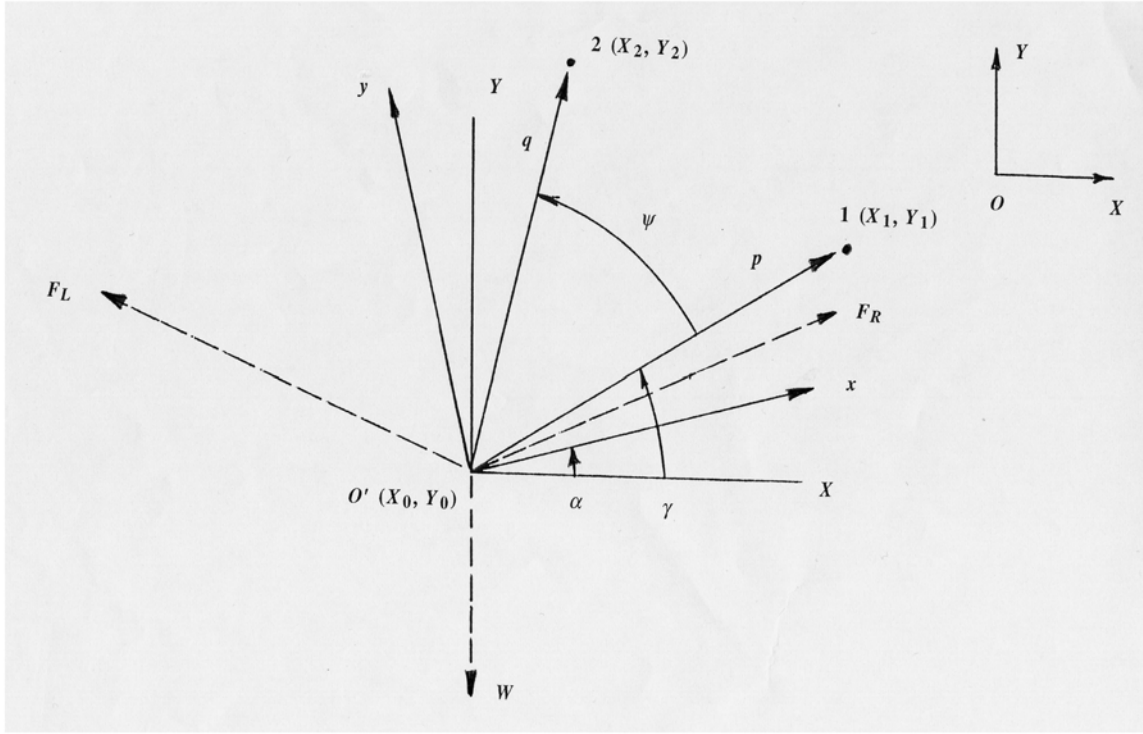

Fig. 8 Reference axes for oil film coefficients

(X_1, Y_1) and (X_2, Y_2) relative to the global axis system X, Y. From these data, the angles α, γ and ψ could be determined, thus locating axes p and q. In general terms these axes were used for reference in defining forces F_p and F_q as follows:

$$F_p = a_{pp}p + a_{pq}q$$
$$F_q = a_{qp}p + a_{qq}q$$

when $\dot{p} = \dot{q} = 0$.

The net rotor loads acting at points O', 1 and 2 were known and could be resolved into components related to the global axes X, Y. The incremental changes could then be transposed to the p and q axes as follows

$$\Delta F_{p1} = \frac{\Delta F_{x(1\text{-}0)}\sin(\psi+\gamma) - \Delta F_{y(1-0)}\cos(\psi+\gamma)}{\sin\psi}$$

$$\Delta F_{q1} = \frac{\Delta F_{x(1\text{-}0)}\cos\gamma - \Delta F_{y(1-0)}\sin\gamma}{\sin\psi}$$

$$\Delta F_{p2} = \frac{\Delta F_{x(2\text{-}0)}\sin(\psi+\gamma) - \Delta F_{y(2-0)}\cos(\psi+\gamma)}{\sin\psi}$$

$$\Delta F_{q2} = \frac{\Delta F_{x(2\text{-}0)}\cos\gamma - \Delta F_{y(1-0)}\sin\gamma}{\sin\psi}$$

Lengths p and q could also be obtained from the X, Y coordinates and for small incremental changes be defined as Δp and Δq. Thus, by rearranging the force equations above, displacement coefficients could be produced as follows

$$a_{pp} = \frac{\Delta F_{p1}}{\Delta p}, \qquad a_{qp} = \frac{\Delta F_{q1}}{\Delta p} \qquad \text{for } q = 0$$

$$a_{qq} = \frac{\Delta F_{q2}}{\Delta q}, \qquad a_{pq} = \frac{\Delta F_{p2}}{\Delta q} \qquad \text{for } p = 0$$

Coefficients related to the p–q axes could be converted to refer to any perpendicular axes x–y as follows

$$a_{xx} = \frac{(a_{pp}\sin\phi - a_{pq}\sin\theta)\cos\theta + (a_{qp}\sin\phi - a_{qq}\sin\theta)\cos\phi}{\sin\psi}$$

$$a_{xy} = \frac{(a_{pq}\cos\theta - a_{pp}\cos\phi)\cos\theta + (a_{qq}\cos\theta - a_{qp}\cos\phi)\cos\phi}{\sin\psi}$$

$$a_{yx} = \frac{(a_{qp}\sin\phi - a_{qq}\sin\theta)\sin\phi + (a_{pp}\sin\phi - a_{pq}\sin\theta)\sin\theta}{\sin\psi}$$

$$a_{yy} = \frac{(a_{qq}\cos\theta - a_{qp}\cos\phi)\sin\phi + (a_{pq}\cos\theta - a_{pp}\cos\phi)\sin\theta}{\sin\psi}$$

where θ is the angle from the chosen x axis to the p axis and is given by $\theta = \gamma - \alpha$, and ϕ is the angle from the chosen x axis to the q axis, given by $\phi = \psi + \gamma - \alpha$. The equations are valid for angles and directions in all quadrants, but Parkins [**7**] predicted uncertainties of about 30 per cent for some directional velocity coefficients when the angle ψ was reduced to 16° or so. For this project, adjustments for the hydrodynamic bearings were equalized end to end and data for the two hydrodynamic bearings were averaged and related to the longitudinal centre of the rotor assembly.

A specially written computer program processed transducer DVM readings into displacements of the rotor at the axial centre-lines of the hydrodynamic bearings and hydrostatic bearing as appropriate. It also resolved the applied force sets (including rotor weight) producing the equilibrium load net force and direction, and the incremental changes between positions O' to 1 and O' to 2, all with reference to the global axes X, Y. The program then formulated the $p-q$ axis reference frame, location angles and displacements and transposed the incremental forces to the $p-q$ axes and determined the related displacement coefficients. These coefficients were then transposed to the perpendicular axes $x-y$, with y aligned parallel tothe static load. The program was thoroughly checked with sample manual calculations. The process could be repeated with different degrees of adjustment applied equally to the hydrodynamic bearings, or with the hydrostatic bearing acting in isolation, rotating or stationary.

6 SAMPLE TEST RESULTS

Following commissioning, running-in trials and calibration exercises, the test rig was used extensively in studying the practical performance of the adjustable hydrodynamic bearings and the hydrostatic bearing in static mode. It is hoped that full results for both types of bearing will be fully reported. By way of indication, however, Tables 1 to 3 show some significant results.

It can be seen that values of displacement coefficients are of the magnitudes and range expected of a fluid film bearing. Table 1 shows that, for zero load, the hydrodynamic bearing stiffness as indicated by the displacement coefficients can be changed by adjustment. In general, the direct coefficients could be increased while retaining significant indirect coefficient values. This would have the effect of suppressing instabilities that may occur, for example at low loads. These characteristics were predicted by theoretical studies carried out with a comprehensive computer model [**8**]. For the hydrodynamic bearing these increases in displacement coefficient values with increased adjustment settings can be equated to the increases in displacement coefficients observed or predicted in conventional bearings with increased eccentricities [**9**].

Table 2 shows that lubricant flowrates remained reasonably constant with loads and adjustments. Table 1 indicates an increase in temperature rise with adjustment, concomitant with the decreased minimum oil film thickness. The continuous adjustment capability was also clearly evident from the oscilloscope trace pictures, with repeatable and reversible adjustments to rotor position being obtained during operation.

Table 3 shows that the hydrostatic bearing, when supporting the stationary rotor, exhibited a pattern of displacement coefficients including significant values for the cross-terms,

Table 2 Lubricant flowrates—hydrodynamic bearing

Adjustment*	Rotor load, W (N)	Rotor speed (r/min)	Lubricant flowrate (ml/s)
Zero	375.7	Zero	28.1
Zero	375.7	3500	21.5
Small	Zero	3500	24.7
Medium	Zero	3500	23.0

*For adjustment C_r, see Table 1.

Table 3 Experimentally derived displacement coefficients—hydrostatic bearing (rotor load $W = 0$, rotor speed $= 0$)*

Supply pressure (kPa)	F_1 (N)	F_2 (N)	a_{xx} (MN/m)	a_{xy} (MN/m)	a_{yx} (MN/m)	a_{yy} (MN/m)
1379.0	98.1	98.1	69.5	−6.3	115.6	36.9
1379.0	196.2	196.2	61.7	−25.4	89.9	50.5
1723.8	98.1	98.1	65.3	−56.7	84.7	34.2
1723.8	196.2	196.2	68.1	−95.0	81.6	117.0

*$C_r = 0.051$ mm at pocket lands.

Table 1 Experimentally derived displacement coefficients—hydrodynamic bearing (rotor load $W = 0$, rotor speed = 3500 r/min)

Adjustment*	F_1 (N)	F_2 (N)	a_{xx} (MN/m)	a_{xy} (MN/m)	a_{yx} (MN/m)	a_{yy} (MN/m)	ΔT (K)
Zero	98.1	98.1	104.1	−22.9	104.8	2.2	29.2
Zero	147.2	147.2	206.0	−15.7	218.2	14.5	30.9
Zero	196.2	196.2	70.2	−29.7	188.8	215.0	32.4
Small	98.1	98.1	207.5	6.1	303.6	102.3	27.1
Small	392.4	392.4	203.6	−64.2	107.1	119.7	33.8
Medium	98.1	98.1	125.0	23.5	−125.0	273.5	36.0
Medium	392.4	392.4	292.5	−8.7	238.3	179.6	38.5
Large	196.2	196.2	218.0	−92.2	−132.7	350.9	36.6

*Zero adjustment $C_r = 0.03$ mm; small adjustment $C_r = 0.019$ mm; medium adjustment $C_r = 0.013$ mm; large adjustment $C_r = 0.008$ mm.

a_{yx} and a_{xy}. A hydrostatic bearing when operating with no contribution from hydrodynamic action derives its stiffness principally by the pocket pressures generated externally in conjunction with the effects of the restrictors when the geometry (i.e. the clearances) alter with changes in load. It is conceivable, therefore, that a change in one direction might have an effect on pocket pressures in a direction at right angles, as the clearances will alter in this direction too, although this point is not addressed in commonly used design empirical models.

7 OBSERVATIONS ON THE USE OF THE TEST RIG

Specific problems were experienced with oil exits, heat dissipation and instrumentation sensitivity. A central oil gallery drain in the central shaft was not very successful, despite some vacuum assistance. It was clear that the majority of the oil left the bearing via the outer ends of the rotor. This led to some oil spray and spillage loss. For some tests with the hydrodynamic profile adjustments in play, the rotor displacements were very small and the inductive displacement transducers were operating in a relatively small portion of their effective linear range.

A satisfactory means of determining the stationary shaft centre in warmed-up conditions was not found. This was due to the rapid change in temperatures when the rotor was slowed to a halt, the difficulties in applying known repeatable motions to the non-rotating rotor and the likelihood of small, but significant, thermal distortions occurring to the rotor bore if it contacted the warmed-up shaft with no lubricant film present. These situations would have been met when determining data to locate the fixed shaft centre. There was also some risk of damage to the rotor white metal surface with hydrodynamic bearing adjustments applied without such film lubrication. The measurement techniques devised, however, did not require actual location of this centre directly, thus avoiding the problem.

The use of large electromagnets to apply loads to the rotor proved to be very successful. A resultant load in any direction could be set in a matter of seconds, knowing beforehand the required components. Total capacity was limited to a rated 1 kN, but in practice each electromagnet could sustain a steady force of 1.9 kN with one particular control transformer unit, and of 1.7 kN with the other. It was also noted that some cross-interference occurred whenever one force component setting was altered, requiring fine adjustments to both magnet control settings each time a change was made.

A large number of tests were carried out successfully, and confidence was gained in the general trends of operational characteristics observed. With the adjustable hydrodynamic bearings, the rotor was shown to adopt a rotational centre position that could be moved on demand, or be reset to the original equilibrium position after the load had been changed. The tests were repeated for both end bearings and for different speeds, and the same effects were observed. The bearing continued to support the applied loads during all adjustments. These characteristics have potential benefits in improving the accuracy of location of the proposed grinding wheel design. Additional characteristics were observed relating to the stiffness of a stationary hydrostatic bearing.

Overall, the test rig, as a multi-body dynamics system, met the objectives of its design, and it is believed to be the first of its kind to demonstrate the continuous adjustment capability of the novel bearing concept. The principle and lessons learnt were subsequently applied to a larger conventionally oriented bearing which demonstrated similar characteristics [**10**].

8 CONCLUSIONS

A novel form of test rig has been designed and built whereby a driven rotor is supported via fluid film bearings on a stationary central shaft. Full film lubrication was generated for all rotor speeds including zero.

A means was devised and implemented to apply rotor loads, and adjust their magnitudes and directions, quickly by non-contacting means.

Measurement techniques were adopted to include rotor radial position measurement by non-contacting means and derive oil film displacement coefficients by incremental loading and consequent changes of rotor position. For the hydrodynamic bearing, general results and trends observed closely followed those predicted by a comprehensive theoretical model and further tests on a large form of bearing. For the hydrostatic bearing, results reflected trends reported for other orientations of bearing, extended for stationary conditions.

The test rig design, comprising various bodies and components interacting directly, provided a useful facility to demonstrate a number of key characteristics of a novel hydrodynamic bearing concept, and for a stationary hydrostatic bearing. Experience gained has subsequently been applied to other forms and sizes of adjustable bearing.

ACKNOWLEDGEMENTS

The author is pleased to acknowledge the assistance of Dr D.W. Parkins and the support of Cranfield University, the Open University and BTG International Limited.

REFERENCES

1 **Martin, J. K.** and **Parkins, D. W.** Fluid film bearings. International (PCT) Pat. Application WO–95/29346, BTG International Limited, London, 1995.
2 **Morrison, D.** Influence of plain journal bearings on the whirling action of an elastic rotor. *Proc. Instn Mech Engrs*, 1962, **176**(22), 542–553.
3 **Martin. J. K.** Investigations into an adjustable fluid film bearing. PhD thesis, Cranfield University, 1997.

4 Martin, J. K. Extended expansion of the Reynolds equation. *J. Engineering Tribology*, 2002, **216**(J1), 49–51.

5 Magnetic materials. Parts 1 to 10. BS 6404, British Standards Institution, 1984.

6 Specification for white metal bearing ingots. BS 3332, British Standards Institution, 1987.

7 Parkins, D. W. Measurement of oil film journal bearing damping coefficients—an extension of the selected orbit technique. *Trans. ASME, J. Tribology*, 1995, **117**, 696–701.

8 Martin, J. K. and **Parkins, D. W.** Theoretical studies of a continuously adjustable hydrodynamic fluid film bearing. *Trans. ASME, J. Tribology*, January 2002, **124**(1), 203–211.

9 Rowe, W. B. and **Chong, F. S.** Computation of dynamic force coefficients for hybrid (hydrostatic/hydrodynamic) journal bearings by the finite disturbance and perturbation techniques. *Tribology Int.*, October 1986, **19**, 5.

10 Martin, J. K. and **Parkins, D. W.** Testing of a large adjustable hydrodynamic journal bearing. *Tribology Trans. STLE*, 2001, **44**, 4.